Integrity of hybrid steel-to-composite joints for marine application

S W Boyd[1]*, **J I R Blake**[1], **R A Shenoi**[1] and **A Kapadia**[2]
[1]School of Engineering Sciences, University of Southampton, Southampton, UK
[2]Composite Technology Centre, VT Group (Halmatic), Portsmouth, UK

Abstract: There are many instances where the use of weight-saving polymer composite material for an entire structure is either too complex, too expensive or unfeasible. In these circumstances the use of a hybrid structure can incorporate the benefits of traditional (e.g. steel) construction coupled with the advantages of composite materials [e.g. glass-reinforced polymers, glass-reinforced plastic (GRP)] in weight-critical areas. A number of studies have been carried out on the static strength of hybrid steel-to-composite joints.

In the present study, an experimental investigation was undertaken into the fatigue life characterization of a hybrid steel-to-GRP joint. It was found that the fatigue data correlated well with the statistical-based Weibull cumulative distribution function. In addition, post fatigue (in-plane and out-of-plane) residual strength tests were undertaken to ascertain the joint structural performance after cyclic loading. Finite-element-based progressive damage analyses incorporating damage initiation and propagation characteristics, showed good correlation with experimental results.

Keywords: composite materials, hybrid steel-to-composite joints, fatigue life characterization, residual strength tests

1 INTRODUCTION

The application of hybrid metal-to-composite structures has been gaining momentum over the last number of years and their use can be found in a widening number of engineering disciplines. One initial use of metal-to-composite joints was in the repair of aluminium space frames with composite patches in the aerospace industry. With the large amount of experience in this field [**1**–**4**], the study of composite hybrid joints has been extended to applications in the land transport [**5**, **6**] and marine industries [**7**–**9**].

In the marine industry, reduced hull and superstructure weight increases payload for the same speed and power requirements and additionally allows for a more stable and effective operations platform for naval ships where seakeeping may be one of the prime objectives. Feasibility studies into the construction of composite superstructures for naval vessels began in the early 1980s [**9**]. Since then there has been increasing interest in the use of composite materials for naval superstructures. The French navy have implemented such a superstructure on their La Fayette class frigate in the form of a helicopter hangar [**7**]. Subsequently there has been increasing research interest in joints between steel and glass-reinforced plastic (GRP) for use in the hull–superstructure and hull–bulkhead joints [**8**, **10**–**11**].

Wright *et al.* [**8**] investigated a fibre-reinforced composite–steel connection for transverse ship bulkheads. These joints were tested in tension, compression, and lateral bending. They found that a suitable connection could be made and that symmetric rather than asymmetric joints provide better strength characteristics.

Clifford *et al.* [**10**] looked at very similar joints in lateral deflection. These specimens allowed investigation into the effect of joint geometry on structural performance, specifically the impact of the length of the steel insert on bending strength. By increasing the length of steel insert penetration into the core material the resulting failure moved from core failure to yielding of the steel.

Cao and Grenestedt [**11**] decreased the penetration of the steel insert in an attempt to both decrease the weight of the hybrid component and to reduce stress concentrations in critical areas. The failure occurred in a

The MS was received on 15 October 2004 and was accepted after revision for publication on 22 November 2004.
** Corresponding author: Fluid Structure Interactions Research Group, School of Engineering Sciences, University of Southampton, Southampton, UK. email: sboyd@ship.soton.ac.uk*

similar manner to that observed by Clifford *et al.* [**10**] with yielding of the steel and shear failure of the core. Overall strength to failure was found to be approximately the same.

In the present study, an investigation is undertaken into the fatigue life characterization of a geometrically similar joint to those used in references [**7**–**11**]. Details of the joint are shown in Fig. 1. Although static and dynamic (shock/blast) loadings are of great importance, especially in naval vessels, it is assumed that the vessel must survive and operate for its required service life. This involves withstanding extremes of temperature and humidity cycling commonly found when operating in the Gulf/temperate regions and the day-to-day marine environment loadings such as accelerations due to wave motions. It is the latter that is discussed in the present research as being the prime generator of cyclic loading within the ship structure.

In addition, the residual strength of the joint, which is critical in terms of through-life ability of a vessel to withstand large instantaneous loading, is assessed in both axial compression and lateral externally applied bending. In-plane residual strength testing was carried out after fixed intervals of cyclic loading and out-of-plane residual strength was examined for differing fatigue crack lengths.

Numerical simulation of the static behaviour is undertaken incorporating progressive damage tools. The model is analysed using the ABAQUS suite of finite element (FE) software using Fortran-based user subroutines to implement the progressive damage analysis. Failure criteria for isotropic materials are used to identify initial failure and material property degradation is implemented to simulate the non-linear load–deflection behaviour observed in the experimental results.

2 JOINT DESIGN PHILOSOPHY

The hybrid joint used in the present study, shown in Fig. 1, is based on the design for the hangar to weather deck connections (Fig. 2) currently in service in the French navy on the La Fayette class frigates. The original joint was manufactured using hand lay-up techniques with a polyester resin. It was felt that the use of resin infusion would be an improvement both in quality of the final product and ease of mass production.

2.1 Materials

The materials used in the present study are a 3×1 twill weave 780 g/m^2 E-glass woven roving (Chomarat 800S4), vinylester resin (Dow Derakane 411–C50), 150 kg/m^3 balsa wood core (Baltek AL600–10 Contourcore) and 6 mm thick mild steel (D55).

The steel was delivered in its 'black' form, i.e. it had no weld-through primer on it. The steel surface was pre-treated by shot blasting to SA2.5 standard, using chilled iron grit, G24. The steel was then acetone wiped to

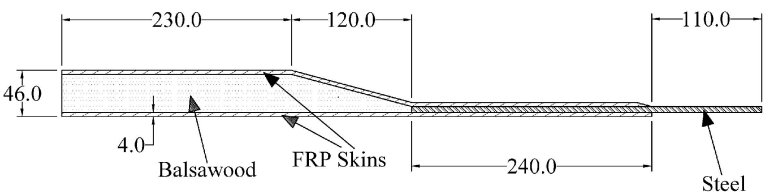

Specimen Thickness: 100mm

Fig. 1 Details of the hybrid joint used in the present study

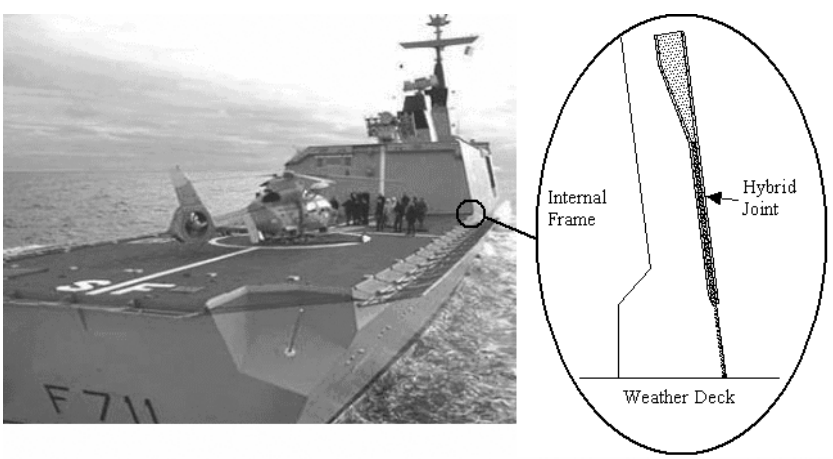

Fig. 2 Helicopter hangar on the French La Fayette class frigate (picture reproduced courtesy of DCN)

remove any debris from the blasting operation. Once the acetone had evaporated the steel was primed using catalyzed Derakane 411–45 vinylester resin. The resin was applied using a brush and the application was carried out within 4 h of shot blasting (generally accepted as an owner's requirement for paint).

2.2 Specimen manufacture

The initial step of the manufacturing process involves the surface preparation of the steel as described in section 2.1. It is generally accepted that shot blasting the bond surface prior to bonding is the most suitable method to prepare the steel for adhesive bonding.

The manufacture of the specimens was carried out as follows:

1. Apply release agent to the tool surface.
2. Lay-up distribution mat and peel-ply.
3. Lay-up eight layers of glass using adhesive spray to prevent movement of the reinforcement layers.
4. Lay-up steel and balsa.
5. Lay-up eight layers of glass using adhesive spray to prevent movement of the reinforcement layers.
6. Lay-up peel-ply, distribution mat and vacuum bag. Do not seal vacuum bag until the day of the infusion.
7. Apply 0.1 bar vacuum and ensure that reinforcement cloth is smooth and that balsa meets steel.
8. Ensure ambient temperature is above 16 °C.
9. Carry out a vacuum integrity test by applying 1 bar of vacuum and hold for 10 min. if any significant loss in vacuum (>0.07 bar) then check seal.
10. Pour resin, catalyst and accelerator into a clean bucket and mix well.
11. Release inlet and outlet clamps and allow resin to infuse the lay-up.
12. Once the resin has gelled, clamp resin inlet and leave under vacuum for 6 h.
13. Allow infusion to cure overnight and de-bag and de-mould sample.

3 EXPERIMENTAL SET-UP

3.1 Boundary conditions

It was important when testing the specimens to represent, as much as possible, the loading scenario that would be found in the full-scale structure. Due to the asymmetric geometry of the joint (Fig. 1) any load applied as a compressive force through the axis of the steel would produce a lateral bending force due to load eccentricity. Given that the design requirements on a naval vessel preclude excessive flexibility in this direction, it was felt that this was not representative of how the structure would behave in the real environment—the joint would be prevented from bending in this manner due to the internal framing of the superstructure. Figure 3 shows schematically how

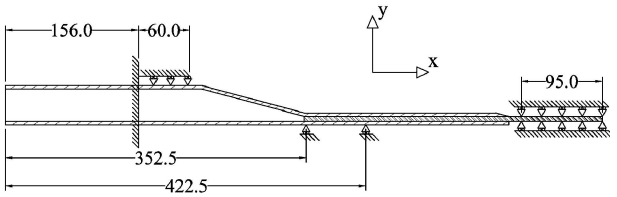

Fig. 3 Boundary conditions of the experimental specimen

the specimen was constrained and loaded. In order to prevent the lateral bending, denoted in Fig. 3 by a deflection in the negative *y*-direction, a system of anti-bending guides was positioned near the steel/balsa interface. With the knowledge that fatigue tests were to be carried out in the future using the same experimental set-up, it was a concern that positioning rollers the length of the specimen to remove the lateral deflection could result in overworking of the joint through friction. While one roller would reduce the lateral deflection at the point at which it would be positioned, two rollers would ensure that the steel end of the specimen would remain in-axis, representing the boundary conditions anticipated in-service more accurately.

The positions of the anti-bending guides were calculated using an FE analysis. The analysis involved observing the negative *y*-deflection for various roller positions. Initially the rollers were positioned equal distances either side of the steel/balsa interface (Fig. 4a). This resulted in the steel deflecting at its tip around the first of the rollers. It was observed that this roller position would lead to excessive peel forces at the steel/balsa/GRP interface resulting in premature failure. In order to prevent such bending of the steel, the rollers were positioned so as to support only the steel portion of the joint. This dramatically reduced the deformation at the rollers (Fig. 4b). Figure 5 shows the final position of the anti-bending guides.

3.2 Applied loads

The load was applied via a hydraulic ram controlled by an Instron 8800 controller. The ram was capable of producing 130 kN at maximum hydraulic pressure. Specific load was defined via a 250 kN load cell.

In the present study a compressive force was felt to be the most likely loading scenario encountered in the real structure. On a naval vessel, the use of this particular joint has direct application to the problem of mounting a lightweight GRP superstructure (typically a helicopter hangar) to a steel deck (Fig. 2). It is assumed that the hangar structure does not contribute to the global bending strength of the hull girder due to its length being considerably smaller than the overall length of the hull, and it is decoupled from the hull girder due to the differences in elastic modulus of the materials used for the hull and hangar. Therefore, only forces induced by

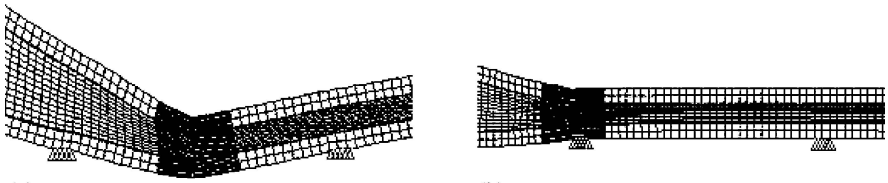

Fig. 4 (a) Anti-bending guides equidistant from steel/balsa interface (scaled deflection). (b) Anti-bending guides supporting only the steel (scaled deflection)

Fig. 5 Position of anti-bending guides

the structure's own weight and accelerations due to motion are considered significant. With the vessel at rest and in calm water, the joint will experience only a compressive force equal to the apportioned weight of the hangar structure and any ancillary equipment mounted on it. The generation of tensile forces on the other hand, while unlikely, is not inconceivable. When the vessel is underway and is sailing in seas rather than calm water, it will experience motions in all six degrees of freedom. These motions translate to the connection between the hull of the vessel and the hangar superstructure. Assuming the hangar is located on the after-deck of the ship, for the connection to experience a tensile load or at most a relief of the compression loading due to the hangar's structural weight, the aft end of the ship needs to experience one negative g for weightlessness or greater for tensile load. This scenario would be possible if the aft end of the ship were in free fall from coming off the back of a wave, but in reality this is highly unusual.

It is feasible that either the port or starboard side of the structure would be subjected to one or more negative g during roll. The size of the tensile force would be related to the position of the neutral axis of the hangar structure and the roll rate, but again it is highly unlikely that one negative g will be experienced in reality and only a combination of roll and heave may in extreme circumstances produce enough acceleration to cause the structure to be weightless.

From the discussion of realistic loading scenarios described above, the most likely force to be encountered by the hybrid metal composite joint is, therefore, compressive and to this end the testing of the fatigue life of the joint has been carried out in compression.

3.3 Test programme

The first phase of testing of the hybrid joint is to determine the ultimate static compressive strength of the joint. This will identify the maximum load amplitude for the fatigue test phase.

Fatigue life characterization of the hybrid joint at various load amplitudes in compression load cycles is carried out in the second test phase. A zero-compression test allows for the most extreme form of cyclic compression loading for a given mean load level and the greatest flexibility in the choice of load amplitude. Through characterizing the fatigue life, the endurance limit of the hybrid joint can be determined as well as identifying the number of cycles (N) to failure for the subsequent axial (loading applied in the plane of the steel insert) residual strength tests.

The third test phase investigates the residual strength of the hybrid joint. Two tests were carried out in this phase. The first was an axially compressive residual strength test where specimens were prepared by fatigue cycling to a fraction of the total number of cycles to failure for a given load amplitude. The second residual strength test was carried out in fully encastred four-point bending where, in this instance, the specimens were prepared by fatigue cycling axially at a fixed load amplitude to produce cracks of differing lengths.

4 RESULTS

4.1 Static testing

The specimens tested for static strength were loaded under position control to pick up any stress relief, the rate of deflection set to approximately 0.5 mm/min. Ultimate compressive failure occurred at 108 kN. It is known that any axially loaded joint will develop high stress concentrations at the ends of the jointed region. In the present study additional stress concentration will be present due to the load eccentricity and subsequent

internal bending (global bending has already been removed by the anti-bending guides). Thus, it is assumed that the most highly stressed region of the joint should be located at the steel/balsa interface and in particular on the flat side. It is in this region that the initial crack was observed. The crack then propagated along the steel/GRP interface on the flat side. It is expected that the cause of the initial crack is due to peel forces caused by the load path eccentricity. This crack extends due to mode I crack opening until the anti-bending guides are approached. From this point on the crack extends due to mode II shearing of the adhesive layer.

The load–deflection curve of ultimate compressive failure can be seen in Fig. 6. The ultimate compressive strength (UCS) of the joint is 108 kN, however for the purpose of maximum cyclic load levels, a nominal compressive strength (UCS_{nom}) is taken as 100 kN. The nominal value of ultimate compressive strength was chosen due to limited numbers of specimens for experimental testing statically. The 100 kN UCS_{nom} provides a conservative limit for maximum cyclic load levels and equates to an expected experimental scatter level of 8 per cent.

4.2 Fatigue life characterization

The fatigue life characterization tests carried out in this phase of the programme are outlined in Table 1. The first tests described in Table 1 were designed to assess the structural response of the joint over a long period of time, allowing for a careful observation of anticipated crack growth, stiffness degradation and energy dissipation. The lack of existent data available on these joints and the very limited number of specimens available for a pure fatigue analysis (i.e. without the residual strength testing) meant that the test matrix had to be evolutionary in nature.

During the tests, data on the load and deflection of the specimen were acquired for one cycle in every 100. The resulting output data were analysed to investigate any stiffness degradation during the fatigue life. The stiffness of the joint was obtained by fitting a straight line to the hysteresis loop of the load–deflection curve and obtaining the gradient. In addition, the area inside the hysteresis loop is plotted against the number of cycles. A change in this area indicates a release of energy, possibly due to damage within the joint [**12**].

Tests 1 and 2, from Table 1, were carried out at relatively low loads and load amplitudes. After 10^6 cycles at 1 Hz test 1 was stopped. There were no visual indications of damage. The joint was tested to failure under axially compressive static load. The resulting strength was 100 per cent of the UCS. In addition, and shown in Fig. 7, there was no significant loss in stiffness or dissipation of energy, both of which can be a measure of damage. The implication of tests 1 and 2 is that in order to obtain fatigue failure of the hybrid joint, higher mean load levels and/or higher load amplitudes would be required.

Specimen 13a (test 3) was subjected to a load amplitude of 43 kN, equivalent to 0–86 per cent of the UCS_{nom}. Figure 8 shows the stiffness change and energy release against number of cycles and unlike the low amplitude/low mean load levels of tests 1 and 2, there is a significant loss in stiffness and a corresponding increase in energy release prior to ultimate failure at approximately 1700 cycles.

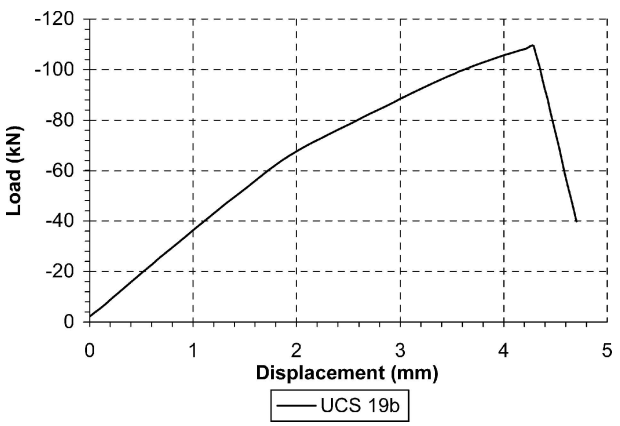

Fig. 6 Static compression load–deflection curve

Table 1 Fatigue test programme

Test No.	Description	Specimen	Load amplitude (kN)
1	17–34% UCS_{nom}	12a	8.6
2	34–69% UCS_{nom}	12b	17.2
3	0–86% UCS_{nom}	13a	43.0
4	0–69% UCS_{nom}	14a	34.4
5	0–60% UCS_{nom}	14b, 15a	30.1
6	0–51% UCS_{nom}	13b	25.8
7	0–77% UCS_{nom}	15b, 16a	38.7

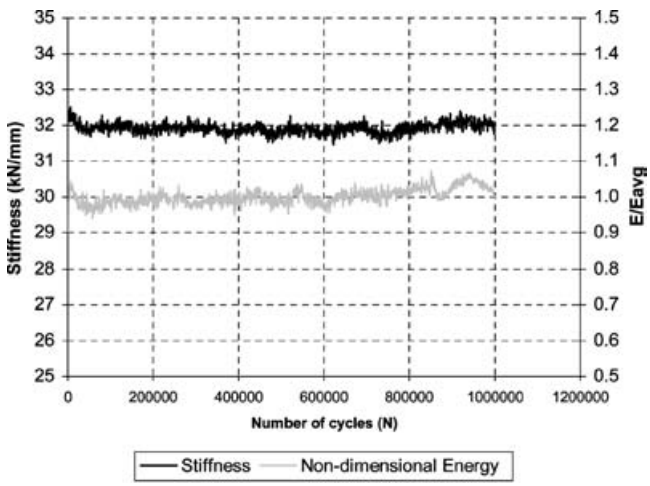

Fig. 7 Stiffness and energy results versus number of cycles for 17–34 per cent of UCS_{nom}

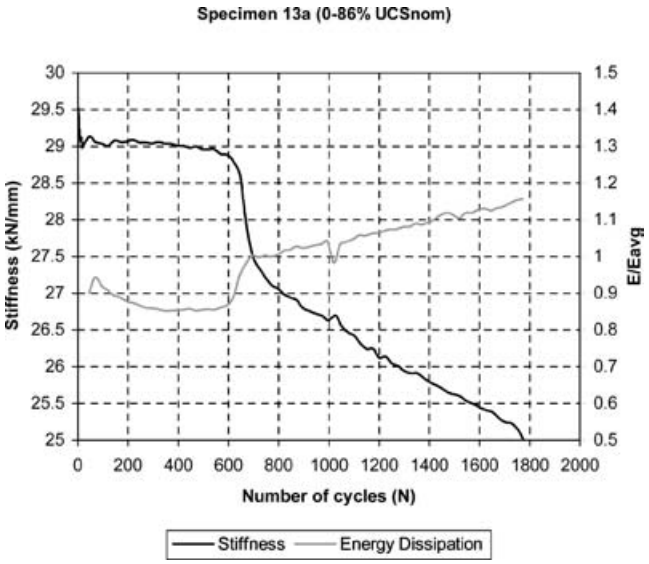

Fig. 8 Stiffness and energy dissipation of specimen 13a under 0–86 per cent UCS_{nom} fatigue cycle

The load amplitude of the fatigue tests was systematically reduced in order to obtain the fatigue endurance limit. Tests were carried out at load amplitude P_a equal to 38.7 kN, 34.4 kN, 30.2 kN and 25.8 kN. The stiffness and energy plots for all these tests exhibit a loss in stiffness and corresponding increase in energy release during their fatigue life. However, while higher load amplitudes induced total failure, the specimen subjected to the lowest load amplitude remained intact, albeit with visual signs of failure, past 3.5×10^6 cycles. Given this fact, it was assumed that the fatigue endurance limit of the hybrid joint was at, or close to, a load amplitude of 25 per cent UCS_{nom}.

In addition, the results indicate that the fatigue life of the hybrid joint is dependent on the load amplitude rather than the mean load. The specimen in test 1 was subjected to a load amplitude of 17 per cent UCS_{nom} and a mean load of 26 per cent UCS_{nom}. This applied loading did not appear to cause any damage to the hybrid joint even after 10^6 cycles. In contrast increasing the load amplitude to 26 per cent UCS_{nom} for the same mean load caused visual signs of failure (test 6) after 10^6 cycles. For only a marginal increase in mean load (approximately 30 per cent UCS_{nom}) but with a still greater increase in load amplitude to 30 per cent UCS_{nom} (test 5), complete specimen failure occurred between 10^5 and 10^6 cycles.

Figure 9 shows the fatigue life curve of the hybrid joint in terms of load amplitude P_a and number of cycles ($\log_{10} N$). A representation of the whole life of the joint may be described by a number of discrete functions. Figure 9 shows a discrete logarithmic function representing the experimental data without consideration of the static test case. The level of correlation between the chosen logarithmic function and the experimental data is high, with a variance accounted for value, VAC or R^2, equal to 0.95. A more appropriate and useful function to represent the data would be continuous in nature. A Weibull cumulative density function, $W(N)$, commonly used to describe the fatigue behaviour of composite structures [**13**, **14**] is, therefore, also presented in Fig. 9. The Weibull function is defined from the UCS and is fitted using the shape, β, and scale, η, parameters as described in equation (1). These parameters are selected so as to provide a minimum value of error through the least squares approach. The correlation between the experimental data and the function used to fit the data is very good with an R^2 value also equal to 0.95, validating the use of the Weibull function to describe the as-determined fatigue life of the hybrid joint. It must be noted that the function is based upon a fatigue load endurance limit of 25 per cent of UCS_{nom}. However, a more accurate identification of the endurance limit would be expected to provide a better curve fit to the experimental data.

$$W(N) = \mathrm{UCS} - (\mathrm{UCS} \cdot \mathrm{e}^{-(N/\eta)^{\beta}}) \tag{1}$$

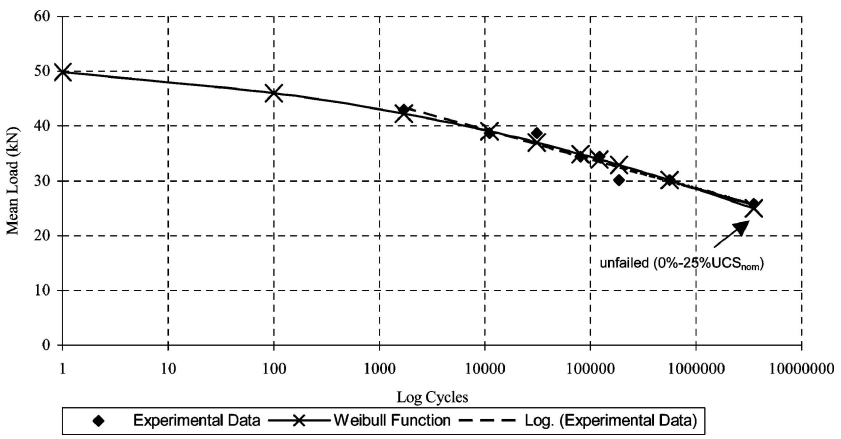

Fig. 9 Fatigue life curve for hybrid joint with respect to mean load

The curve obtained from the present study is typical of those obtained from fatigue characterization of composite materials [**17**]. The goodness of fit of the Weibull cumulative density function provides confidence in predicting the joint life and the corresponding probability density function can predict the probability of failure for any given load amplitude.

4.3 Residual strength testing

Residual strength tests allow the evaluation of remaining strength in a structure after a given life cycle. In the present study the hybrid joint has been subjected to fatigue cycles, equivalent to those used for fatigue life characterization in section 4.2, to represent a portion of the structure's life. Two residual strength tests were performed: in-plane and out-of-plane. The in-plane tests consisted of fatiguing the hybrid joint to a predetermined fraction of its number of cycles to failure, N. The joint was subsequently tested in axial compression to failure. Load and deflection were monitored. The out-of-plane tests involved fatiguing the hybrid joint in order to create a crack in the specimen of a predetermined length. The joint was then tested in four-point bending with fully encastred end conditions as shown in Fig. 10. This loading was chosen to represent an external force applied normal to the surface of the superstructure. The fully encastred end conditions provide a conservative estimate of the lateral residual bending strength of the hybrid joint and were chosen to best represent the boundary conditions expected in the full-scale structure. The steel end would be welded to the weather deck and would most likely incorporate some kind of bracket to provide additional reinforcement. The composite sandwich end would be expected to be attached to a longitudinal stiffener, both of which could be represented by fully clamped end conditions.

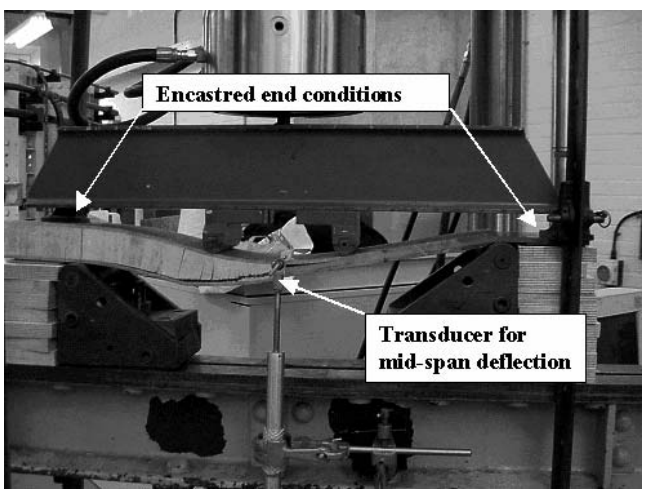

Fig. 10 Out-of-plane residual strength test set-up

It was found in the fatigue life characterization that there was significant scatter in the resultant number of cycles to failure N at a given load amplitude. This led to a lack of confidence in the choice of the N value to be used in the in-plane residual strength tests. This variability in the fatigue behaviour of the hybrid joint resulted in more damage being observed in the specimen tested to one-third ($N/3$) of its N value than the specimen tests to two-thirds ($2N/3$). However, this phenomenon is not represented in the results of the in-plane residual strength tests, where no difference was observed in the residual strength value.

While the in-plane residual strength results are not presented here it was found that the strength of a fatigued specimen was 100 per cent of the static UCS_{nom}, equivalent to 92 per cent of the single compressive strength value obtained in section 4.1, under axial loading. Following the assumption made in section 4.1, once the crack is beyond the second anti-bending guide, crack propagation extends due to mode II shearing. This implies that the shear strength of the adhesive layer dictates the failure load of the joint. Regardless of the number of cycles and extent of visible cracking, residual strength remains dependent on the shear area remaining.

The out-of-plane residual strength tests were performed on specimens containing fatigue cracks of predetermined length. All fatigue cracks were created by cycling with a load amplitude of 34.4 kN (34 per cent of UCS_{nom}) at 1 Hz. The bending tests were carried out using a 100 kN Instron test frame with an 8800 controller. Load, cross-head displacement and mid-span displacement were acquired via a Strawberry Tree data shuttle and DasyLab software. The crack lengths and corresponding residual strength results are presented in Table 2. A graph of initial joint stiffness against crack length is shown in Fig. 11. From this figure there appears to be a trend of stiffness reduction with increasing crack length. Figure 12 shows the full load displacement plot for specimen 22a (50 mm crack length). There are a number of points of stress relief in this graph and these correspond to the specific failures within the joint (description of the events in Fig. 12 are given in Table 3). The out-of-plane failure of the hybrid joint is shown graphically in Fig. 13. The results presented in Table 2 indicate that residual strength remains at 100 per cent regardless of the length of the fatigue crack. However,

Table 2 Out-of-plane residual strength test results

Specimen	Crack length (mm)	Residual strength (kN)	Mid-span deflection (mm)
23a	0	11.4	14.1
22a	50	11.4	12.0
20a	75	11.3	16.0
19b	115	12.7	20.7
23b	145	11.1	13.7

Table 3 Out-of-plane residual strength test events

Event	Observation	Load (kN)	Disp. (mm)
0 to A	Tip of balsa within the taper begins to make cracking sounds as load is increased. The GRP begins to debond from the steel on the taper side at the centre of the joint	0–11.4	0–12.0
A to B	Once the crack on the taper side (steel/GRP interface) exceeds a critical length, load is released as the GRP/balsa interface parts along the length of the taper on the taper side	11.4–7.9	12.0–12.7
B to C	The remaining balsa outside the taper region is put under stress as the load rises	7.9–10.1	12.7–19.9
C to D	The GRP/balsa interface parts along the entire length of the interface on the taper side	10.1–6.9	19.9–22.3
D to E	Load rises over a large increase of displacement as the existing fatigue crack is opened and increased by a further 10 mm	6.9–10.3	23.3–46.2

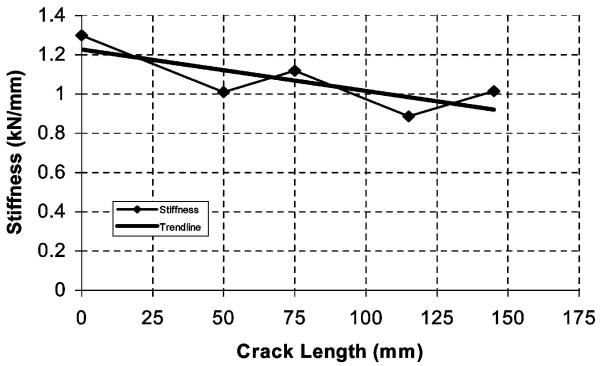

Fig. 11 Initial bending stiffness against crack length

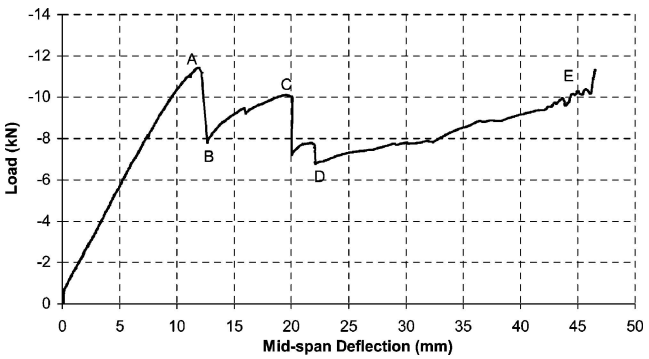

Fig. 12 Load displacement for residual strength test containing a 50 mm crack

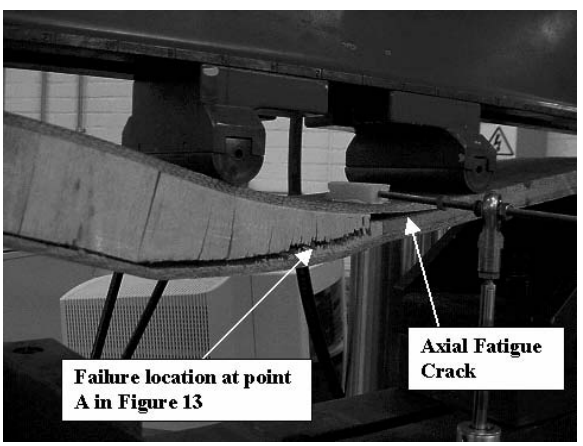

Fig. 13 Failure of joint in four-point bending

due to the joint being fully encastred, the steel near the end clamp yields. This causes a peel stress at the steel end of the GRP overlap on the flat side and begins a debond at this interface. If the fatigue crack were sufficiently long that the fatigue crack and the bending crack resulted in a complete debond of the GRP/steel interface on the flat side, the stiffness and hence the ultimate strength of the joint might be reduced. However, with the fatigue crack tip being sufficiently far away from the end of the overlap, and limitations in the experimental test rig, the two cracks did not converge hence the joints all fail due to a debond between the GRP and balsa on the taper.

5 NUMERICAL MODELLING

In an attempt to more clearly understand the failure mechanisms within the hybrid joint and to observe and predict the damage progression, a numerical model with the facilitation for progressive damage modelling (PDM) was developed. The model analyses the stresses within the increasingly loaded structure and if necessary readjusts local stiffness according to predefined failure criteria. This tool was developed to look at static failure of the joint and to take into account the non-linear nature of the load–deflection relationship observed from experiment.

5.1 General

Numerical modelling of the hybrid joint is carried out using the finite element package ABAQUS 6.2. The joint is divided into four distinct areas: GRP, balsa, steel and the resin-rich layer between the steel and GRP substrates. In the context of this work this resin-rich layer is defined as the adhesive layer. The PDM-user subroutine is only used to define the material properties and stresses for the adhesive layer as it was observed from the experimental tests that the joint failure occurred only in this region.

The mechanical properties of each region are defined in Table 4, where the x, y and z subscripts refer to the in-plane, through thickness and out-of-plane material

Table 4 Material properties for numerical model

	Material			
Property	GRP	Balsa	Adhesive	Steel
E_x (MPa)	20 600	56.951	2944.7	209 000
E_y (MPa)	6770	2965	2944.7	209 000
E_z (MPa)	20 600	56.951	2944.7	209 000
G_x (MPa)	3030	147	–	–
G_y (MPa)	3030	147	–	–
G_z (MPa)	3030	147	–	–
ν_{xy}	0.231	0.01	0.36	0.29
ν_{xz}	0.171	0.23	0.36	0.29
ν_{yz}	0.231	0.24	0.36	0.29
σ_T (MPa)	–	–	50	–

directions of the laminate, respectively. The model is constructed using eight-node quadrilateral, solid elements. Due to the joint's geometry the analysis has been simplified into a two-dimensional (2D) plane stress with thickness problem. The boundary conditions for the numerical model were kept as close as possible to those used experimentally, see Fig. 2.

5.2 Linear response

A linear analysis was conducted to assess the correlation between initial experimental and numerical stiffness of the joint. The hybrid structure was subjected to a global displacement of 4.5 mm with a resultant load of 150 kN, considerably higher than the failure load achieved experimentally. However, good correlation between experimental and numerical stiffness was achieved in the linear region. There was a clear point of divergence between the results at a deflection of approximately 2.0 mm. Based on this result it was felt that a non-linear material model would take into account the loss in global stiffness of the joint at higher deflections.

In addition the linear model has been used to increase understanding of the failure mechanisms of the hybrid joint. It was observed during the experimental results that failure, during the in-plane testing, proceeded along the flat side of the joint at the interface between the steel and the GRP from the centre to the steel end. The linear numerical model indicates that the area of highest stress is concentrated at the same location. By introducing a progressive damage model the path of failure can be modelled and compared with that observed experimentally.

For the out-of-plane residual strength numerical model the location of the major stress concentration is also located at the interface of the steel, GRP and balsawood on the flat side. By removing a given number of resin elements in the adhesive layer to represent the presence of a fatigue crack, the stress concentration re-locates in the adhesive as the debonds appear. With just the fatigue crack on the flat side of the GRP/steel interface the major stress concentration is located at the GRP/steel interface on the taper side. Once the crack extends along this interface the major stress concentration moves to the GRP/balsa interface on the taper side. This is the location of the first of the stress relief events described in Table 3. Figure 14 shows the location of the stress concentration in the numerical model with cracks on both GRP/steel interfaces.

5.3 Non-linear material model

Implementation of the non-linear material model involved the inclusion of a 'user subroutine' to define material properties and hence stresses in each of the elements of interest.

For any chosen Young modulus and Poisson ratio used to define the isotropic nature of the adhesive layer, the incremental stress can be calculated using the equation

$$\{\sigma\}_N = [\mathbf{C}]_N \{\varepsilon\}_N \tag{2}$$

where N is the increment number and $[\mathbf{C}]$ is the constitutive matrix of material properties. The total stress in the element is given by

$$\{\sigma\}_{\text{total}} = \sum_{i=1}^{N} \{\sigma\}_i \tag{3}$$

5.3.1 *Damage modelling*

In order to assess any possible damage to the adhesive layer due to incremental loading the resultant stresses obtained from equation (2) can be analysed using well-known failure criteria for isotropic materials such as maximum stress/strain, maximum shear stress or shear strain energy theories.

In the present study the shear strain energy theory, more commonly known as the von Mises failure criteria [**15**], is used. This states that failure will occur if the strain energy exceeds the strain energy at failure under

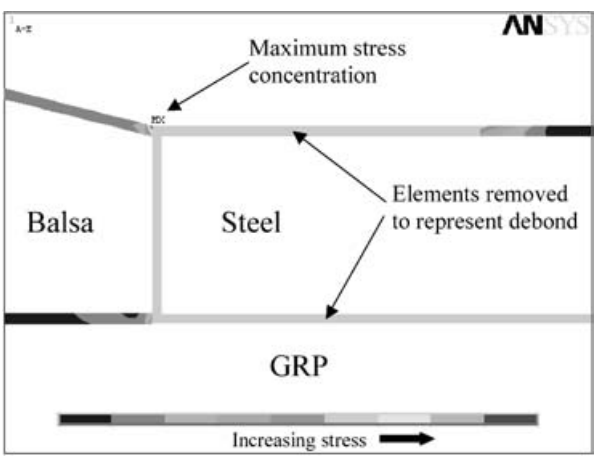

Fig. 14 Position of major stress concentration after steel/balsa interface failure in four-point bending

simple tension and from basic theory [**16**] is defined as

$$\sqrt{\sigma_1^2 + \sigma_2^2 - \sigma_1\sigma_2} \geqslant \sigma_t \quad (4)$$

where σ_1 and σ_2 are the major and minor principal stresses, respectively, and σ_t is the tensile strength of the resin used in the adhesive layer. In the present study the tensile strength of the resin is used to evaluate failure according to equation (4) and is given in Table 4.

5.3.2 Material property degradation

It can be stated for all but the most brittle materials that, when the stress in a material causes the failure criteria to be exceeded, the reduction in material properties is not instantaneous. Tests carried out to British Standard BS 2782 (Part 3, Methods 320A–320F) were conducted on bulk castings of the adhesive. The results indicate that the adhesive does not behave in a purely brittle manner. Historically there are three commonly used material degradation models: instantaneous [**17**], gradual [**18**] and constant stress [**19**]. The examination of the global stiffness reduction of the hybrid joint appears to tend toward a gradual reduction model. However, in order to define this scenario within the user subroutine of material property definition, the gradual reduction method results in a negative Young modulus, ultimately causing numerical problems associated with the global finite element equations. To overcome this the stress in the element is reduced to represent a negative Young modulus. This can be carried out using either a linear or non-linear reduction model.

By investigating the effect of differing functions for stress reduction using a piecewise linear system, an approximation to the true function can be identified. Three points can be determined from knowledge of the strain in each element at the point at which the failure criteria are exceeded. The first point is where the initial failure criteria are exceeded and the third is the complete failure point. The middle point defines the approximate function shape (see Fig. 15).

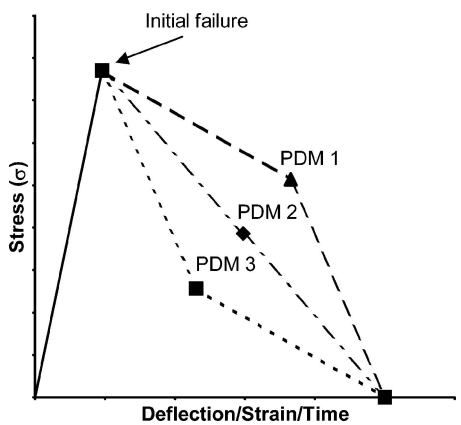

Fig. 15 Stress reduction models

5.4 Numerical results

It should be noted that progressive cracks may have an effect on the behaviour of the structure: this is modelled normally using fracture mechanics principles. In the context of this paper, however, the focus is on strength issues and failure based on strength methods and criteria. The results obtained from the numerical model are given in Fig. 16. This graph shows the experimental load–deflection curve compared with a linear finite element result and three non-linear results. The non-linear results have used the three differing stress reduction models as shown in Fig. 15.

As discussed in section 5.2, there is a clear point of divergence between the predicted linear response and experimental observation at 2 mm deflection. The non-linear PDM successfully identifies this point of divergence for all three stress reduction models. Furthermore, beyond a global displacement of 2 mm the correlation between the presented non-linear numerical results and the experimental result, depending on the choice of post-failure material function (see Fig. 15), represents a compromise between excellent prediction of failure load and excellent prediction of failure strain.

The progressive damage model clearly indicates the path of failure in the joint as the stresses in the adhesive layer combine to exceed the failure criteria. Figure 17 shows the position of the first point of failure of the joint. Its location is at the interface of the steel, balsawood and GRP on the flat side of the hybrid joint. It is in this location that the first experimentally observed crack occurs, subsequently leading to the GRP/steel debond. In the case of the tested specimens subsequent increased loading led to crack propagation along the flat side in the steel/GRP interface. The numerical model successfully identified this phenomenon.

6 CONCLUSIONS

In this study the fatigue life for a hybrid steel-to-GRP joint has been characterized. It was found that a Weibull cumulative density function correlated well with experimental data for the hybrid joint, a function commonly associated with the description of the fatigue life of composite materials. Confident use of the Weibull function in relation to the structural performance of the hybrid joint allows for fatigue life prediction and determination of the probability of failure for a given load amplitude.

The axial residual strength tests carried out on the hybrid joint indicate that damage caused by in-plane fatigue loading has little influence on the ultimate failure load of the joint in axial compression. In addition there is very little reduction in stiffness of the joint observed in lateral bending with increasing axially induced fatigue damage.

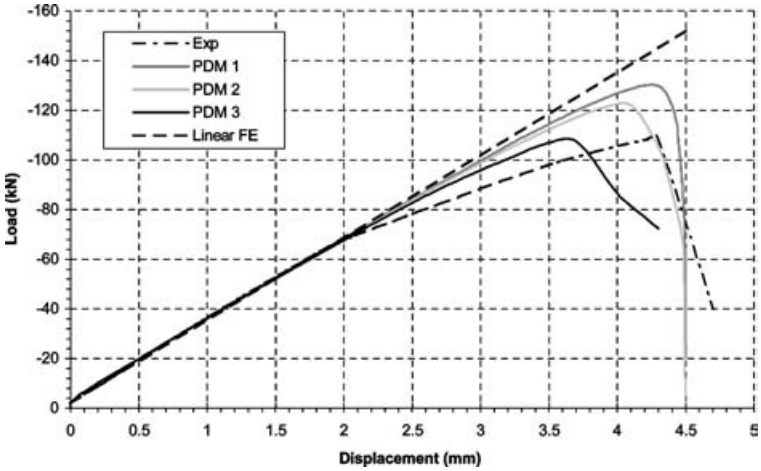

Fig. 16 Numerical versus experimental load–deflection curves

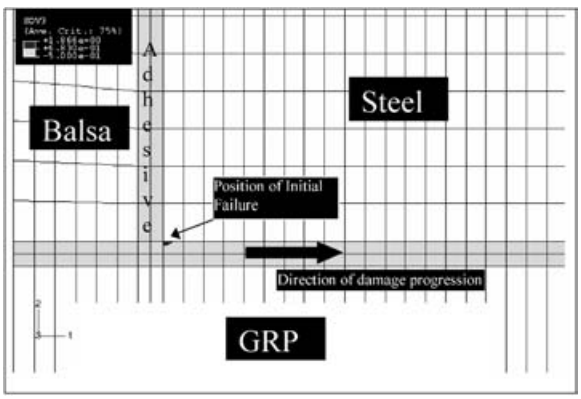

Fig. 17 Position of initial failure and direction of damage propagation (within adhesive layer at the interface between GRP/steel/balsa, flat side of specimen)

The numerical analyses provide insight into the failure mechanisms present in the hybrid joint. The linear analysis indicated a very good correlation of experimental and numerical joint stiffness for the linear portion of the load–deflection curve. The progressive damage model accurately represented the displacement at which the load–deflection curve becomes significantly nonlinear.

The progressive damage model, in association with the three presented stress reduction models provided and depending on the choice of stress reduction model, provides excellent agreement with experiment of either failure load or failure strain. Continuing investigation into more appropriate stress reduction models would lead to a better compromise between prediction of both ultimate failure load and strain.

ACKNOWLEDGEMENTS

The authors gratefully acknowledge the EUCLID RTP3.21 Programme and the UK Ministry of Defence for funding of this research. Discussions with project partners, particularly colleagues at QinetiQ, Vosper Thornycroft (VT), University of Newcastle upon Tyne and Det Norske Veritas (DNV) have been very beneficial to the authors' work.

REFERENCES

1 **Baker, A.** Repair of cracked or defective metallic aircraft components with advanced fibre composites—an overview of Australian work, *Composite Structure*, 1984, **12**, 153–181.

2 **Baker, A., Chester, R., Davis, M., Roberts, J.** and **Retchford, J.** Reinforcement of the F-111 wing pivot fitting with a boron/epoxy doubler system—materials engineering aspects, *Composites*, 1993, **24**, 511–521.

3 **Ong, C. L.** and **Shen, S. B.** Some results on metal and composite patch reinforcement of aluminium honeycomb panel, *Theor. Appl. Fracture Mech.*, 1991, **16**(2), 145–153.

4 **Naboulsi, S.** and **Mall, S.** Characterisation of fatigue crack growth in aluminium panels with a bonded composite patch, *Composite Structs*, 1997, **37**(3/4), 321–334.

5 **Shin, K. C., Kim, Y. G., Lee, D. G.** and **Choi, J. M.** Adhesively bonded lap-joints for composite-steel shell structure of high-speed vehicles, *Composite Structs*, 1997, **38**(1–4), 215–227.

6 **Choi, J. H.** and **Lee, D. G.** Torque capacity of co-cured tubular lap joints, *J. Composite Mater.*, 1997, **31**(14), 1381–1396.

7 **Le Lan, J. Y., Parneix, P.** and **Gueguen, P. L.** Composite material superstructures, International Conference on *Nautical Construction with Composite Materials*, Paris, France, 1992.

8 **Wright, P. N. H., Wu, Y.** and **Gibson, A. G.** Fibre reinforced composite-steel connections for transverse ship bulkheads, *Plast., Rubb. Composites*, 2000, **29**(10), 549–557.

9 **Mouritz, A. P., Gellert, E., Burchill, P.** and **Challis, K.** Review of advanced composite structures for naval ships and submarines, *Composite Structs*, 2001, **53**, 21–41.

10 **Clifford, S. M., Manger, C. I. C.** and **Clyne, T. W.** Characterisation of a glass-fibre reinforced vinylester to

steel joint for use between a naval GRP superstructure and a steel hull, *Composite Structs*, 2002, **57**(1–4), 59–66.

11 **Cao, J.** and **Grenestedt, J. L.** Test of a redesigned glass-fibre reinforced vinyl ester to steel joint for use between a naval GRP superstructure and a steel hull, *Composite Structs*, 2003, **60**, 439–445.

12 **Shenoi, R. A., Read, P. J. C. L.** and **Hawkins, G. L.** Fatigue failure mechanisms in fibre-reinforced plastic laminated tee joints, *Int. J. Fatigue*, 1995, **7**(6), 415–426.

13 **Burman, M.** and **Zenkert, D.** Fatigue of foam core sandwich—1: undamaged specimens, *Int. J. Fatigue*, 1997, **19**(7), 551–561.

14 **Lee, J., Harris, B., Almond, D. P.** and **Hammett, F.** Fibre composite fatigue—life determination, *Composites Part A*, 1997, **28A**, 5–15.

15 **von Mises, R.** Mechanik der fasten Koerper im plastisch deformablen Zustand, *Goettinger Nachrichten, Math-Phys*, 1913, 582.

16 **Megson, T. H. G.** *Structural and stress analysis*, 1996 (Arnold, London, UK).

17 **Murray, Y.** and **Schwer, L.** Implementation and verification of fibre-composite damage models, *Failure Criteria and Analysis in Dynamic Response*, 1990, AMD 107, pp. 21–30 (ASME).

18 **Petit, P. H.** and **Waddoups, M. E.** A method of predicting the nonlinear behavior of laminated composites, *J. Composite Mater.*, 1969, **3**, 2–19.

19 **Hahn, H. T.** and **Tsai, S. W.** On the behaviour of composite laminates after initial failures, *Astronaut. Aeronaut.*, 1983, **12**, 58–62.

